JACS
JOURNAL OF THE AMERICAN CHEMICAL SOCIETY

Article

pubs.acs.org/JACS

Synergy between Two Metal Catalysts: A Highly Active Silica-Supported Bimetallic W/Zr Catalyst for Metathesis of *n*-Decane

Manoja K. Samantaray,* Raju Dey, Santosh Kavitake, Edy Abou-Hamad, Anissa Bendjeriou-Sedjerari, Ali Hamieh, and Jean-Marie Basset*

King Abdullah University of Science & Technology, KAUST Catalysis Center (KCC), 23955-6900 Thuwal, Saudi Arabia

Supporting Information

ABSTRACT: A well-defined, silica-supported bimetallic precatalyst [≡Si−O−W(Me)$_5$≡Si−O−Zr(Np)$_3$] (**4**) has been synthesized for the first time by successively grafting two organometallic complexes [W(Me)$_6$ (**1**) followed by ZrNp$_4$ (**2**)] on a single silica support. Surprisingly, multiple-quantum NMR characterization demonstrates that W and Zr species are in close proximity to each other. Hydrogenation of this bimetallic catalyst at room temperature showed the easy formation of zirconium hydride, probably facilitated by tungsten hydride which was formed at this temperature. This bimetallic W/Zr hydride precatalyst proved to be more efficient (TON = 1436) than the monometallic W hydride (TON = 650) in the metathesis of *n*-decane at 150 °C. This synergy between Zr and W suggests that the slow step of alkane metathesis is the C−H bond activation that occurs on Zr. The produced olefin resulting from a β-H elimination undergoes easy metathesis on W.

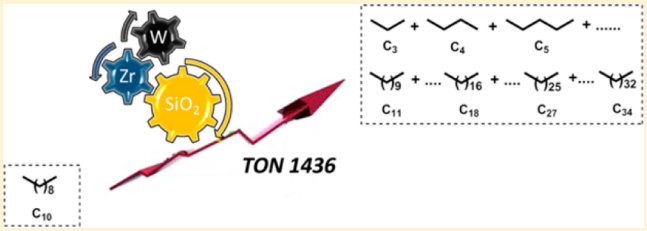

INTRODUCTION

Alkanes, which are the major constituents of petroleum, have gained intense research interest in the past few years.[1−4] Despite recent advances in synthesizing well-defined,[3,5] highly active catalysts for conversion of alkanes, many aspects need to be addressed for the commercialization of these catalysts. One of them is improving the turnover number (TON). The primary constraint of alkane metathesis is the intrinsic low reactivity of C−H and C−C bonds of paraffin.[6] Alkane metathesis, which is believed to be an ultimate solution to petrochemicals, consists of mainly three different chemical transformations, namely, dehydrogenation of alkanes, olefin metathesis, and hydrogenation of newly formed olefin.[7] In 1973, Burnett and Hughes first discovered a dual tandem catalytic system comprising Pt/Al$_2$O$_3$ for dehydrogenation/hydrogenation and WO$_3$/SiO$_2$ for the olefin metathesis reaction.[8] Though this dual catalytic system had an impact on the conversion of alkanes, it suffers from high reaction temperature (450 °C). Recently, Goldman and Brookhart et al. reported a tandem catalytic system that consists of two homogeneous catalysts for alkane metathesis at a lower temperature (125−175 °C).[9,10] While in 1997, using a surface organometallic chemistry approach, our group reported a well-defined, multifunctional, silica-supported tantalum hydride catalyst, which is able to convert alkanes at much lower temperature (150 °C).[11] After this breakthrough, various supported metal catalysts based on Ta, Mo, and W were employed for the alkane metathesis.[12−17] However, these catalytic systems showed little success in terms of efficiency,[17−20] until the recent development of silica and silica−alumina-supported W(Me)$_6$, which have been proven to be efficient in alkane metathesis with significantly higher TONs.[21,22] In the quest for improving the efficiency in the alkane metathesis reaction, we intentionally planned to move from a monometallic system (tungsten) to a bimetallic system, wherein another metal (1) should be very efficient for dehydrogenation and hydrogenation reactions at 150 °C and (2) should not react with our parent metathesis catalyst. In this context, we decided to use Zr(Np)$_4$ because silica-supported [≡Si−O−Zr(Np)$_3$] has already been reported by us and was fully characterized at the molecular level using solid-state NMR, IR, elemental analysis, and gas quantification methods. The corresponding [(≡Si−O−)$_{4-x}$Zr(H)$_x$] is known to be very active in the hydrogenolysis and C−H bond activation reaction.[23,24]

Herein, we disclose the synthesis and molecular level characterization of a well-defined, silica-supported bimetallic precatalyst [≡Si−O−W(Me)$_5$≡Si−O−Zr(Np)$_3$] (**4**) (Scheme 1), which upon thermal treatment at 100 °C transforms to a mixture of methylidyne species (**5**) (Scheme 2). Precatalyst **4** was converted into its corresponding hydrides by treatment with hydrogen at room temperature for **6** and at high temperature for **7** (Scheme 3). To evaluate its catalytic activity toward alkanes, we chose *n*-decane as the substrate for comparison with our previous studies, which showed that a maximum TON of 350 can be achieved by using a silica−alumina-supported W(Me)$_6$ system. These bimetallic catalysts **4**, **6**, and **7** showed TONs of 1005, 1436, and 1250, respectively, representing a significant increase in activity for

Received: May 4, 2016
Published: June 1, 2016

DOI: 10.1021/jacs.6b04307
J. Am. Chem. Soc. 2016, 138, 8595−8602

Scheme 1. Synthesis of Supported [≡Si−O−W(Me)$_5$≡Si−O−Zr(Np)$_3$] (4)

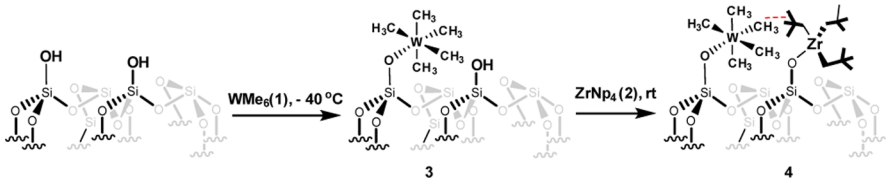

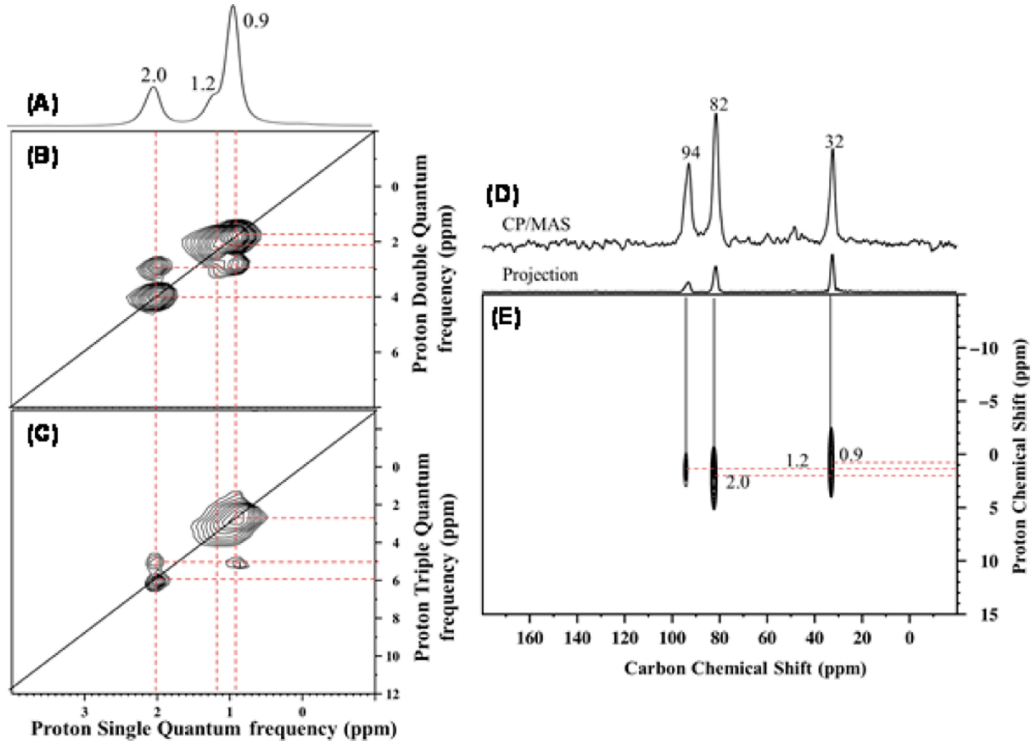

Figure 1. (A) One-dimensional ^{1}H MAS solid-state NMR spectrum of **4** acquired at 600 MHz (14.1 T) with a 22 kHz MAS frequency, a repetition delay of 5 s, and 8 scans. (B) Two-dimensional ^{1}H−^{1}H double-quantum/single-quantum (SQ) and (C) ^{1}H−^{1}H triple-quantum/SQ NMR spectra of **4** (both acquired with 32 scans per t_1 increment, 5 s repetition delay, 128 individual t_1 increments). (D) ^{13}C CP/MAS NMR spectrum of **4** (acquired at 9.4 T (f_0(^{1}H) = 400 MHz) with a 10 kHz MAS frequency, 10 000 scans, a 4 s repetition delay, and a 2 ms contact time). Exponential line broadening of 80 Hz was applied prior to Fourier transformation. (E) 2D ^{1}H−^{13}C CP/MAS dipolar HETCOR spectrum of **4** (acquired at 9.4 T with 10 kHz MAS frequency, 3000 scans per t_1 increment, a 4 s repetition delay, 64 individual t_1 increments, and a 0.2 ms contact time). For all spectra depicted here, only W−Me in **4** was 50% ^{13}C labeled.

the metathesis of *n*-decane. Notably, we have never observed any decomposition of the bimetallic catalyst during the grafting onto the silica support.

RESULTS AND DISCUSSION

Preparation and Characterization of [≡Si−O−W(Me)$_5$≡Si−O−Zr(Np)$_3$] (4) on SiO$_{2-700}$. Individual grafting of W(Me)$_6$ (**1**) and ZrNp$_4$ (**2**) on silica was already reported by us and was fully characterized at the molecular level using solid-state NMR, IR, elemental analysis, and gas quantification methods.[21,25] For the first time, we anchor the homogeneous organometallic species **1** followed by **2** on a single surface [SiO$_{2-700}$, which contains 0.3 ± 0.1 mmol silanol groups per gram] at −40 and 25 °C, respectively, under an inert atmosphere of argon (Scheme 1).

The elemental analysis shows that **4** contains 1.13 wt % of tungsten and 0.37 wt % of carbon (C/W ratio = 5 ± 0.1, expected value of 5), and 1.9 wt % of zirconium and 3.73 wt % of carbon (C/Zr ratio = 14.94 ± 0.1, expected value of 15).

An IR spectrum of **4** showed the complete disappearance of the bands at 3747 cm^{-1}, which are associated with isolated and geminal silanols. For **4**, two new groups of bands in the region of 3018−2864 and 1465 and 1365 cm^{-1} were observed. These are assigned to ν(CH) and δ(CH) vibrations of the methyl and the neopentyl ligands bonded to tungsten and zirconium (Supporting Information Figure S1).

Further spectroscopic analyses of **4** were also conducted with solid-state NMR. The ^{1}H magic-angle spinning (MAS) solid-state NMR spectrum of **4** displays three signals at 2.0, 1.2, and 0.9 ppm (Figure 1A). Strong autocorrelation peaks were observed at 0.9 and 2.0 ppm in double-quantum (DQ) (1.8 and 4.0 ppm in indirect dimensions) and in triple-quantum (TQ) (2.7 and 6.0 ppm in indirect dimensions) NMR experiments under 22 kHz MAS, as shown in Figure 1B,C, respectively. This strong autocorrelation peak is attributed to the methyl groups, whereas the peak at 1.2 ppm autocorrelates in DQ (2.4 ppm indirect dimensions) but not in TQ, which corresponds to methylene. In addition, and very surprisingly, we also observe correlations outside the diagonal between the methyls of W (2.0 ppm) and methyls of Zr−Np (0.9 ppm), which confirms that both of the moieties are unexpectedly very close to each other in space. The ^{13}C CP/MAS NMR spectrum of an

DOI: 10.1021/jacs.6b04307
J. Am. Chem. Soc. 2016, 138, 8595−8602

Scheme 2. Thermal Treatment of Species 4 Leads to Formation of Tungsten Methylidyne on the Surface

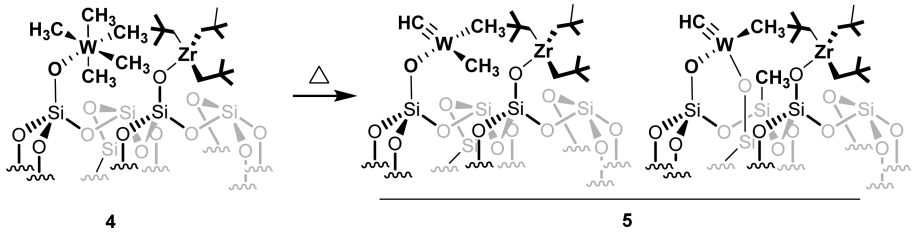

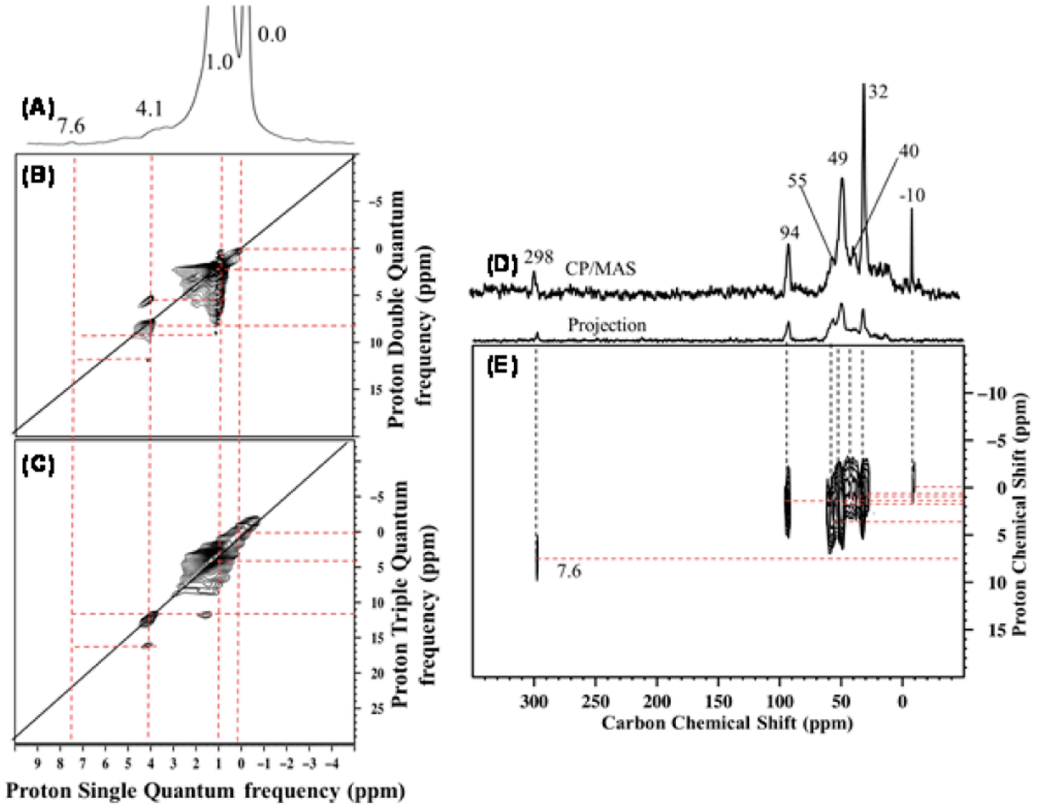

Figure 2. (A) One-dimensional ^{1}H spin−echo MAS solid-state NMR spectrum of $[(\equiv SiO)_xW(\equiv CH)Me_y]$ after maintaining the temperature of 50% ^{13}C labeled **2** at 345 K for 6 h (acquired on a 600 MHz NMR spectrometer under a 20 kHz MAS spinning frequency, number of scans = 8, repetition delay = 5 s). (B) Two-dimensional ^{1}H−^{1}H DQ and (C) ^{1}H−^{1}H TQ (acquired on a 600 MHz NMR spectrometer under 22 kHz MAS spinning frequency with a back-to-back recoupling sequence, number of scans = 128, repetition delay = 5 s, number of t_1 increments = 128). (D) ^{13}C CP/MAS NMR spectrum (10 kHz MAS at the same field as above, number of scans = 20 000, repetition delay = 4 s, contact time = 2 ms, line broadening = 80 Hz). (E) Two-dimensional ^{1}H−^{13}C CP/MAS dipolar HETCOR NMR spectrum acquired with short contact times of 0.2 ms under 10 kHz MAS (number of scans per increment = 3000, repetition delay = 4 s, number of t_1 increments = 32, line broadening = 80 Hz).

enriched sample of **4** (please note that only tungsten methyls are 50% enriched) showed three peaks at 82, 94, and 32 ppm (Figure 1D) that correlate, respectively, with the proton resonances at 2.0, 1.2, and 0.9 ppm, as indicated in the 2D ^{1}H−^{13}C HETCOR NMR spectrum recorded with a contact time of 0.2 ms, assigned to methyls of W and neopentyls of zirconium (Figure 1E). The ^{1}H and ^{13}C chemical shifts are similar to those observed in the solution NMR spectra of molecular species **1** and **2** (Supporting Information Figures S2−S6). Note that the grafting of the mixture of **1** and **2** on oxide supports could result in the formation of monopodal or bipodal grafted species due to strained silica ring defects produced after thermal dehydroxylation. However, ^{1}H and ^{13}C solid-state NMR spectroscopy did not indicate the presence of a signal at or near 0.0 ppm, which cancels the probability of methyl or neopentyl transfer to an adjacent silicon atom of silica and hence rules out the formation of bipodal species $[(\equiv Si{-}O)_2W(Me)_4(\equiv Si{-}O)_2Zr(Np)_2]$ [≡Si−R, R = Me or Np].

Synthesis of the well-defined W/Zr bimetallic catalyst on a silica surface $[\equiv Si{-}O{-}W(Me)_5\equiv Si{-}O{-}Zr(Np)_3]$ (**4**) was our main purpose to enhance the catalytic properties of the catalyst. To observe the effect of the bimetallic system on catalysis, initially, we employed **4** for the metathesis of *n*-decane. To our expectation, it proved to be very active in *n*-decane metathesis with a TON of 1005 compared to a TON of 150 using **3**,[22] clearly indicating the cooperative role of Zr in the metathesis of *n*-decane.

Observation of Tungsten Carbyne Species 5 via Thermal Treatment of Precursor 4. The excellent activity observed using catalyst precursor **4** might be due to the formation of tungsten methylidene species in the surface as it is covered by two metal complexes. We heated supported species **4**, which is 50% enriched by ^{13}C of tungsten methyl from 298

DOI: 10.1021/jacs.6b04307
J. Am. Chem. Soc. 2016, 138, 8595−8602

to 345 K. When the temperature was held at 345 K for 6 h, several peaks were observed (Supporting Information Figure S7). The ^{1}H NMR resonances of neopentyl of zirconium at 0.9 and 1.2 ppm did not change, whereas the peak at 2.0 ppm diminished and several other signals were observed. The NMR spectra of the converted material suggested that the products are W-methyl/methylidyne species **5** (Scheme 2 and Figure 2). The ^{1}H NMR of the converted material exhibits several new signals at 0.0, 1.0, 1.1, 4.1, and 7.6 ppm (Figure 2 and Supporting Information Figure S7). The signals at 1.0, 1.1, and 4.1 ppm autocorrelate in the 2D DQ and TQ ^{1}H−^{1}H homonuclear dipolar correlation spectra and are assigned to different methyl groups of tungsten (Figure 2B,C).

Along with this observation, we also observe that the proton resonance at 7.6 ppm displays no autocorrelation in the DQ and TQ spectra (Figure 2B,C). The broad signal at 0.0 ppm is assigned to methane and methyl groups transferred to silica (i.e., ≡SiMe, suggesting a bipodal W/silica), which is supported by an autocorrelation in DQ and TQ (Figure 2B,C).

The ^{13}C CP/MAS NMR spectrum (Figure 2D) displays new signals at 40, 49, and 55 ppm, a signal at 298 ppm at high frequency, and a signal at −10 ppm at low frequency in addition to the stable signals at 32 and 94 ppm. Additionally, the 2D ^{1}H−^{13}C HETCOR NMR spectrum (Figure 2E) with a short contact time (0.2 ms) shows a correlation between the methyl protons (1.1 and 1.0 ppm) and that of carbon atoms (49 and 40 ppm), and a correlation between the methyl protons centered at 4.0 ppm and the carbon at 55 ppm allows the assignment of the carbon−proton pairs to the individual methyl groups. Furthermore, the strong correlation between the carbon and proton signals at 298 and 7.6 ppm, respectively, strongly supports the assignment of a methylidyne moiety (W≡CH) (based on our previous studies on [≡SiO)W(≡CH)Me$_2$], Figure 2E).[21] In addition, two strong correlations are observed in the 2D ^{1}H−^{13}C HETCOR proton at 0.9 and 1.2 ppm to that of carbon atoms 32 and 94 ppm, respectively, which are coming from the methylene and methyl moiety of the neopentyl attached to zirconium (Figures 1 and 2E). Furthermore, a correlation in DQ/SQ NMR spectrum between the ≡SiMe at 0.0 ppm and the methyl groups at 4.1 ppm supports the transfer of a methyl group to the silica and suggests the formation of bipodal species (^{13}C, 55 ppm; ^{1}H, 4.1 ppm) (Scheme 2). Since no correlation with the other two methyl groups is observed, these two inequivalent methyl groups (^{13}C, 44 and 40 ppm; ^{1}H, 1.4 and 1.1 ppm) can be assigned to the monopodal species. The methyl groups of both species of **5** correlate with the methylidyne moiety, as observed in both DQ and TQ NMR experiments (Figure 2B,C).

We could not observe the formation of tungsten methylidene during the thermal decomposition stage, but we observed very high reactivity in the metathesis reaction. Therefore, we assumed that we might have been generating zirconium hydride during the reaction. To validate our assumption, we thought to mix both on two different silica (700) supports of tungsten and zirconium hydride separately and carry out our catalytic reaction. Surprisingly, after mixing both supported hydrides and carrying out the catalytic reaction, we observed a slight increase in the rate of the reaction, with a TON of 898 instead of 650 for W hydride alone. However, the TON was observed to be slightly lower than that of **4** (TON = 1005) and **5** (TON = 963). This clearly indicates that having W and Zr both together on the same support favors the metathesis reaction. With this hypothesis, we thought we would synthesize both tungsten and zirconium hydride on the single surface and use them for the catalytic reaction and hence the comparison of the catalyst.

Hydrogenation of Species 4 [≡Si−O−W(Me)$_5$≡Si−O−Zr(Np)$_3$] at Different Temperatures and Their Catalytic Activity. Our previous study showed that we can generate tungsten hydride at room temperature because of its reactive nature toward hydrogen.[26] We thought to react **4** [≡Si−O−W(Me)$_5$≡Si−O−Zr(Np)$_3$] with hydrogen at room temperature to generate tungsten hydride−zirconium neopentyl on silica without forming silicon hydride and then to heat it at 150 °C to generate both the hydride species. In contrast, while passing dry hydrogen through our sample and monitoring the generation of hydride, surprisingly, we observed tungsten and zirconium hydride simultaneously at room temperature (Scheme 3 and Figure 3).

Scheme 3. Formation of the Bimetallic Hydride Species at Different Temperatures

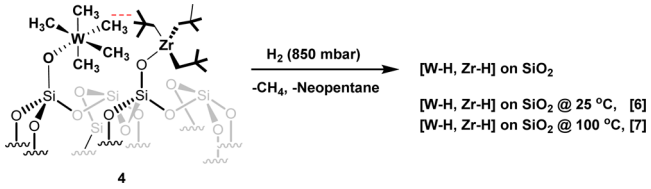

The infrared spectrum shows that the peak intensity decreases at 3018 to 2863 cm^{-1}, and at the same time, four new peaks are observed in the region of 2256 to 1632 cm^{-1}. The peaks at 2200 and 2256 correspond to silicon mono- and bishydride [m, ν(SiH) and ν(SiH$_2$)],[27] and the other two peaks at 1957 and 1632 cm^{-1} represent tungsten hydride ν(WH$_x$) and zirconium hydride ν(ZrH and ZrH$_2$), respectively (Figure 3). ^{1}H NMR shows four major peaks at 1.0, 4.5, 10.9, and 13.3 ppm. The broad peak at 1.0 ppm comes from the unreacted neopentyl groups of zirconium. The new broad peak at 4.5 ppm is ascribed to SiH, SiH$_2$, and the peak at 10.9 ppm is assigned to zirconium monohydride as is already described in the literature.[27] Along with these peaks, we also observe another peak at 13.3 ppm; we believe it might be due to the formation of W−H$_x$ because a literature report showed that the peak corresponding to W−H can be observed in the region of 12−16 ppm[26,28−30] (Supporting Information Figure S8). To completely remove the neopentyl group from zirconium, we heated **4** at 100 °C for 12 h in the presence of 850 mbar of hydrogen (Figure 3 and Supporting Information Figure S10).

After we continued the heating at 100 °C for 12 h, the peak intensities decreased considerably at 3018−2863 cm^{-1}, along with the complete disappearance of the peaks at 1465 and 1365 cm^{-1}, which are supposed to be δ(CH$_2$, CH$_3$) of the zirconium neopentyl group. Along with the disappearance of these peaks, four new distinct peaks were observed at 2200, 2256, 1960, and 1632 cm^{-1}, which are assigned as silicon monohydride and bishydride (m, ν(SiH) and ν(SiH$_2$), ν(WH$_x$) and zirconium hydride ν(ZrH and ZrH$_2$)).[27] It is also characterized by the ^{1}H NMR peaks at 4.5 ppm, which are assigned to SiH, SiH$_2$ and peaks at 10.4 and 12.2 ppm assigned to (Zr−H and ZrH$_2$), respectively, as it is already known in the literature. The peak at 13.3 ppm is assigned as WH$_x$ according to the literature report.[26,28−30] Formation of both hydrides on a single surface was observed for the first time, along with the formation of a more intense silicon hydride peak at higher temperature

DOI: 10.1021/jacs.6b04307
J. Am. Chem. Soc. 2016, 138, 8595−8602

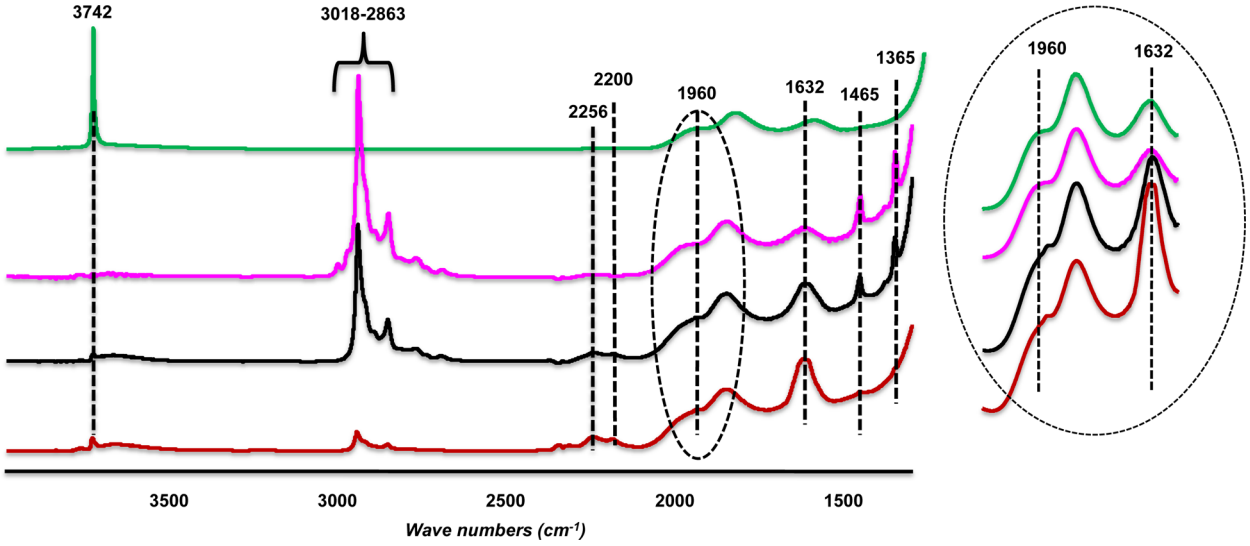

Figure 3. IR spectra of SiO_{2-700} (green) after grafting $W(Me)_6$ and $Zr(Np)_4$ (magenta, **4**). Reaction of **4** with dry hydrogen at room temperature (black, **6**) and after hydrogenolysis at 100 °C (red, **7**).

(Figure 3 and Supporting Information Figure S10). Interestingly, the catalytic results were excellent with these catalysts with the highest TON of 1436 ever observed for a well-defined supported system (Table 1).

Table 1. *n*-Decane Metathesis Reaction: Activity (TON) of Precursors 4, 6, and 7 at 150 °C

catalyst precursor	*n*-decane/W (ratio)	*n*-decane/Zr (ratio)	TON[a]
[W−H@25 °C]	1981		650
[Zr−H@100 °C]		1234	32[b]
[≡Si−O−W(Me)$_5$≡Si−O−Zr(Np)$_3$] (**4**)	4182	1234	1005
[W−H,Zr-H@25 °C] (**6**)	4182	1234	1436
[W−H,Zr-H@100 °C] (**7**)	4182	1234	1250

[a]Turnover number is expressed in mol of *n*-decane converted per mol of tungsten. [b]Turnover number is expressed in mol of *n*-decane converted per mol of zirconium.

Evaluation of the Catalytic Activity of 4, 6, and 7 for *n*-Decane Metathesis. Despite the synthesis of well-defined group V and group VI metal alkyls and their corresponding hydrides on various oxide supports and their use in the alkane metathesis reaction, we did not significantly improve the efficiency in terms of TONs. With this observation of a bimetallic effect, we believe it would be possible to increase the efficiency and hence TON of the catalyst.

Herein, we show the dramatic influence of an auxiliary metal in a bimetallic system for *n*-decane metathesis. Specifically, we chose supporting zirconium hydrides that are well-known for low-temperature C−H bond activation reactions. In this context, we prepared and fully characterized the precatalysts **4**, **6**, and **7**. We tested these catalysts in the *n*-decane metathesis reaction and compared their catalytic activity with that of the existing parent silica-supported catalyst (Table-1).

In a typical experiment, *n*-decane (5.14 mmol) and an appropriate amount of precatalyst **4**, **6**, and **7** (*n*-decane/W = 4182 and *n*-decane/Zr = 1234) were mixed inside a glovebox in a glass ampule. The ampule was frozen outside using liquid nitrogen and sealed under vacuum. Each ampule was heated at 150 °C for a specific time. At the end of the reaction, the ampules were taken outside, frozen under liquid nitrogen, and then quenched with dichloromethane. The reaction mixture was filtered, and the filtrate was collected and was analyzed by GC and GC−MS. The GC chromatogram clearly indicates a wide range of distribution of *n*-alkanes ranging from C_3 to C_{34} (isometathesis) (Figure 4 for precatalyst **6** and Supporting Information Figures S11 and S12 for precatalysts **4** and **7**). NMR studies on the crude sample indicate the formation of only linear alkanes with <1% branched alkanes.

A much wider distribution of products was observed using species **4**−**7**, implying that the double bond isomerization of the olefin intermediate is faster than the overall elementary steps of alkane metathesis (chain-walking process).[31] Additionally, this product distribution also suggests that the hydride species of W and Zr are responsible for double bond migration (via a secondary alkyl), which is being formed during the course of the reaction. Alkane distribution clearly indicates that the formation of lower alkanes is predominant compared to higher alkanes (Figure 4). Similar distribution was already observed by Brookhart and Goldman.[10]

Kinetic studies of *n*-decane metathesis catalyzed by precatalysts **4**, **6**, and **7** were carried out at 150 °C. The conversion versus time curve (Figure 5) indicates that the rate of the reaction for species **6** and **7** is higher than that of species **4**, which is understandable as species **6** and **7** are hydride species generated from species **4**. A steady start was observed in the case of species **6** and **7** at the beginning of the reaction, and at the end, precatalyst **6** was found to be more active and remained stable up to **9** days with the highest conversion of 34% and TON of 1436 (Figure 5). The better performance of species **6** is believed to be due to formation of a lower amount of Si−H, while treatment with hydrogen leads to less bipodal species, compared to species **7** (Figure 3).

We observed that the bimetallic W/Zr system is excellent for the metathesis of *n*-decane, even though only supported zirconium produces fewer metathesis products under identical conditions (conversion 3%, TON = 32) (Table 1). While choosing zirconium to combine with tungsten for a better metathesis result, we envisioned that a supported zirconium is a better catalyst for the C−H activation reaction and it might

DOI: 10.1021/jacs.6b04307
J. Am. Chem. Soc. 2016, 138, 8595−8602

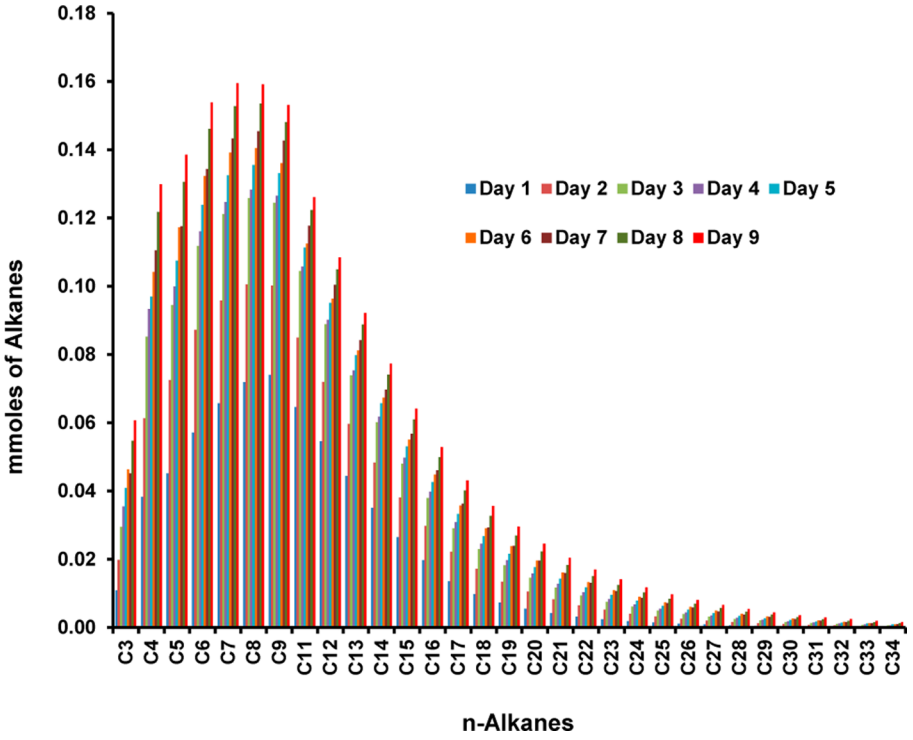

Figure 4. Product distribution of *n*-decane metathesis catalyzed by precatalyst **6**.

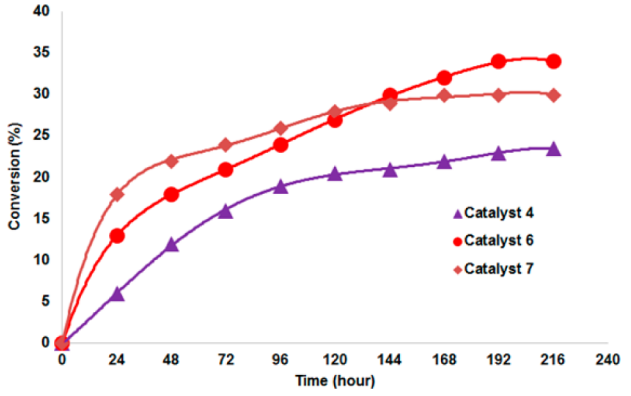

Figure 5. Conversion versus time for the metathesis of *n*-decane catalyzed by [≡Si−O−W(Me)$_5$≡Si−O−Zr(Np)$_3$] (**4**) (purple triangle), [W−H,Zr-H@25 °C] (**6**) (red circle), and [W−H,Zr-H@ 100 °C] (**7**) (brown diamond). Reaction conditions: batch reactor, species **4**, **6**, and **7**, reactant to tungsten ratio 4182, with loading of W (1.1 wt %), *n*-decane (1.0 mL, 5.14 mmol) at 150 °C.

help our tungsten (which is a well-known alkane metathesis catalyst) to improve the reactivity and TON. Additionally, to prove our point, we carried out a reaction of *n*-decane with *tert*-butylethylene (TBE) using supported zirconium at 150 °C. At the end of the reaction, GC and GC−MS data showed the formation of olefin that metathesized with excess TBE and gave 2,2-dimethyldec-3-ene. This above experiment confirms that in the W/Zr bimetallic system the rate and conversion are higher because zirconium forms an olefin and W completes the metathesis and, at the end, reduces the new olefins to alkanes.

CONCLUSION

For the first time, two chemically compatible organometallic complexes were grafted on a single surface (silica 700) without interfering with each other. The surface complex was fully characterized by advanced solid-state NMR, IR elemental analysis, and gas quantification methods. It was observed that at least 50% of zirconium should be near tungsten (strong autocorrelation of the methyls on both systems in ^{1}H−^{1}H double- and triple-quantum spectra). Furthermore, precatalysts **4** and hydrogen-treated species **6** and **7** are proved to be excellent catalysts for the metathesis of *n*-decane with very high TONs compared TONs of their counterparts (silica-supported tungsten methyl and zirconium neopentyls). This opens up new perspectives for the synthesis of various supported bimetallic systems via the surface organometallic chemistry (SOMC) approach to improve the alkane metathesis reaction.

EXPERIMENTAL SECTION

General Procedure. All experiments were carried out using standard Schlenk and glovebox techniques under an inert argon atmosphere. The syntheses and the treatments of the surface species were carried out using high vacuum lines (<10^{-5} mbar) and glovebox techniques. Pentane was distilled from a Na/K alloy under argon and dichloromethane from CaH_2. Both solvents were degassed through freeze−pump−thaw cycles. SiO_{2-700} was prepared from Aerosil silica from Degussa (specific area of 200 m^2/g), which was partially dehydroxylated at 700 °C under high vacuum (<10^{-5} mbar) for 24 h to give a white solid with a specific surface area of 190 m^2/g and containing 0.5−0.7 OH/nm^2. Hydrogen and propane were dried and deoxygenated before use by passage through a mixture of freshly regenerated molecular sieves (3 Å) and R$\bar{3}$−15 catalysts (BASF). IR spectra were recorded on a Nicolet 6700 FT-IR spectrometer using a DRIFT cell equipped with CaF_2 windows. The IR samples were prepared under argon within a glovebox. Typically, 64 scans were accumulated for each spectrum (resolution 4 cm^{-1}). Elemental analyses were performed at Mikroanalytisches Labor Pascher (Germany) and ACL KAUST.

GC measurements were performed with an Agilent 7890A Series (FID detection). We used the following method for GC analyses: column HP-5; 30 m length × 0.32 mm i.d. × 0.25 μm film thickness; flow rate = 1 mL/min (N2); split ratio = 50/1; inlet temperature = 250 °C, detector temperature = 250 °C; temperature program = 40 °C

DOI: 10.1021/jacs.6b04307
J. Am. Chem. Soc. 2016, 138, 8595−8602

(3 min), 40−250 °C (12 °C/min), 250 °C (3 min), 250−300 °C (10 °C/min), 300 °C (3 min); *n*-decane retention time, t_R = 9.6.

GC−MS measurements were performed with an Agilent 7890A series coupled with Agilent 5975C series. GC/MS equipped with a capillary column coated with nonpolar stationary phase HP-5MS was used for molecular weight determination and identification that allowed the separation of hydrocarbons according to their boiling point differences. GC response factors of available C_7−C_{10} *n*-alkane standards were calculated as an average of three independent runs. The plot of response factor versus *n*-alkanes carbon number was determined, and a linear correlation was found; we then extrapolated the response factors for other *n*-alkanes. Organometallic complexes **1** and **2** and their corresponding silica-supported complexes were prepared according to literature procedures.[21,32−34]

Liquid-State Nuclear Magnetic Resonance Spectroscopy. All liquid-state NMR spectra were recorded on Bruker Avance 600 MHz spectrometers. All chemical shifts were measured relative to the residual ^{1}H or ^{13}C resonance in the deuterated solvent: CD_2Cl_2 and C_6D_6.

Solid-State Nuclear Magnetic Resonance Spectroscopy. One-dimensional ^{1}H MAS and ^{13}C CP/MAS solid-state NMR spectra were recorded on Bruker Avance III spectrometers operating at 400 or 600 MHz resonance frequencies for ^{1}H. The 400 MHz experiments employed a conventional double resonance 4 mm CP/MAS probe, while experiments at 600 MHz utilized a 3.2 mm HCN triple resonance probe. In all cases, the samples were packed into rotors under inert atmosphere inside gloveboxes. Dry nitrogen gas was utilized for sample spinning to prevent degradation of the samples. NMR chemical shifts are reported with respect to the external references of tetramethylsilane and adamantane. For ^{13}C CP/MAS NMR experiments, the following sequence was used: 900 pulse on the proton (pulse length 2.4 s), then a cross-polarization step with a contact time of typically 2 ms, and finally, acquisition of the ^{13}C signal under high-power proton decoupling. The delay between the scans was set to 4 s to allow the complete relaxation of the ^{1}H nuclei, and the number of scans ranged between 10 000 and 20 000 for ^{13}C and was 8 for ^{1}H. An exponential apodization function corresponding to a line broadening of 80 Hz was applied prior to Fourier transformation.

The 2D ^{1}H−^{13}C heteronuclear correlation (HETCOR) solid-state NMR spectroscopy experiments were conducted on a Bruker Avance III spectrometer operating at 400 MHz using a 3.2 mm MAS probe. The experiments were performed according to the following scheme: 900 proton pulse, t_1 evolution period, CP to ^{13}C, and detection of the ^{13}C magnetization under TPPM decoupling. For the cross-polarization step, a ramped radio frequency (RF) field centered at 75 kHz was applied to the protons, while the ^{13}C channel RF field was matched to obtain an optimal signal. A total of 32 or 64 t_1 increments with 3000 scans each were collected. The sample spinning frequency was 10 kHz. Using a short contact time (0.2 ms) for the CP step, the polarization transfer in the dipolar correlation experiment was verified to be selective for the first coordination sphere around the tungsten, which led to correlations only between pairs of attached ^{1}H−^{13}C spins (C−H directly bonded).

^{1}H−^{1}H Multiple-Quantum Spectroscopy. Two-dimensional double-quantum and triple-quantum experiments were recorded on a Bruker Avance III spectrometer operating at 600 MHz with a conventional double resonance 3.2 mm CP/MAS probe, according to the following general scheme: excitation of DQ coherences, t_1 evolution, *z*-filter, and detection. The spectra were recorded in a rotor synchronized fashion in t_1 by setting the t_1 increment equal to one rotor period. One cycle of the standard back-to-back recoupling sequences was used for the excitation and reconversion period.[35] Quadrature detection in w_1 was achieved using the states-TPPI method. A MAS frequency of 20 kHz was used. The 90° proton pulse length was 2.5 μs, while a recycle delay of 5 s was used. A total of 128 t_1 increments with 32 or 128 scans each increment were recorded. The DQ frequency in the w_1 dimension corresponds to the sum of two single-quantum frequencies of the two coupled protons and correlates to the w_2 dimension with the two corresponding proton resonances.[27] The TQ frequency in the w_1 dimension corresponds to the sum of the three SQ frequencies of the three coupled protons and correlates to the w_2 dimension with the three individual proton resonances. Conversely, groups of less than three equivalent spins will not give rise to diagonal signals in this spectrum.

Preparation of Supported Complex 4 on SiO_{2-700}. A solution of **1** in pentane (30 mg, 0.11 mmol) was reacted with 2.0 g of Aerosil SiO_{2-700} at −40 °C for 3 h; it was filtered, washed with pentane (3 × 20 mL), and dried for 20 min under vacuum. The resulting light yellow powder was transferred to another double Schlenk tube; to that was added a pentane solution of excess **2** (225 mg, 0.6 mmol) at room temperature, and reaction was continued at that temperature for another 3 h. At the end of the reaction, the resulting light yellow solid was washed with pentane (3 × 20 mL) and dried under dynamic vacuum (<10^{-5} Torr, 1 h). IR data (cm^{-1}): 3018−2863, 1465, 1365. ^{1}H solid-state NMR (400 MHz): δ (ppm) = 2.0 (W−CH_3), 1.2 (Zr−CH_2), 0.9 (−$CH_2(CH_3)_3$). ^{13}C CP/MAS solid-state NMR (100 MHz): δ (ppm) = 94.0 (Zr−CH_2), 82.0 (W−CH_3), 32.0 (Zr−$CH_2(CH_3)_3$). Elemental analysis: W, 0.29−1.13 wt %; Zr, 1.95−1.90 wt %; C, 3.96−4.10 wt %. C/W ratio obtained = 5.0 ± 0.1 (expected was 5); C/Zr ratio obtained = 15.0 ± 0.1 (expected was 15).

Synthesis of 5. In a glass reactor, 1.0 g of **4** was taken and heated at 90 °C (ramped at 60 °C/h) for 12 h to produce a light gray powder, which is a mixture of the monopodal and bipodal species, **5**. IR data (cm^{-1}): 2949−2708, 1467, 1365. ^{1}H solid-state NMR (400 MHz): δ (ppm) = 0.0 (s, Si−CH_3), 0.9 (s, Zr−CH_2−$(CH_3)_3$), 1.0 (s, W−CH_3), 1.1 (s, Zr−CH_2), 1.2 (s, W−CH_3), 4.1 (s, W−CH_3), 7.6 (s, W≡CH). ^{13}C CP/MAS solid-state NMR (100 MHz): δ (ppm) = −10 (Si−CH_3), 32.0 (Zr−$CH_2(CH_3)_3$), 40 (s, W−CH_3), 49 (s, W−CH_3), 55 (s, W−CH_3), 94.0 (Zr−CH_2), 298 (s, W≡CH). Elemental analysis: W, 0.29 wt %; Zr, 2.0 wt %; C, 3.8 wt %. C/W ratio obtained = 3.0 ± 0.1 (expected was 3); C/Zr ratio obtained = 14.3 ±0.1 (expected was 15).

Synthesis of 6. A sample of **4** (100 mg) and dry H_2 (850 mbar) was added in a batch reactor and the reaction allowed to continue at room temperature for 10 h. The light gray product was evacuated at high vacuum and characterized by ^{1}H NMR, IR, and elemental analyses. IR data (cm^{-1}): 2949−2708, 1960, 1632, 1467, 1365. ^{1}H solid-state NMR (400 MHz): δ (ppm) = 1.0 (br, Zr−CH_2−$(CH_3)_3$), 4.5 (br, Si−H, Si−H_2), 10.9 (br, Zr−H_2), 13.3 (s, W−H_x). ^{13}C CP/MAS solid-state NMR (100 MHz): δ (ppm) = 32.0 (Zr−$CH_2(CH_3)_3$), 94.0 (Zr-CH_2). Elemental analysis: W, 0.29 wt %; Zr, 1.98 wt %; C, 1.91 wt %. C/W ratio obtained = 7.3 ± 0.1.

Synthesis of 7. In a reactor tube, 100 mg of **4** was taken, and dry H_2 (850 mbar) was added and heated at 150 °C for 12 h. At the end of the reaction, a dark gray powder was obtained; this product was characterized by ^{1}H NMR, IR, and elemental analyses. IR data (cm^{-1}): 2949−2708 1960, 1632,. ^{1}H solid-state NMR (400 MHz): δ (ppm) = 1.0 (br, Zr−CH_2−$(CH_3)_3$), 1.9 (s, S−OH), 4.5 (br, Si−H, Si−H_2), 10.4 (br, Zr−H), 12.2 (br, Zr−H_2), 13.3 (s, W−H_x). Elemental analysis: W, 0.29 wt %; Zr, 2.01 wt %; C, 0.21 wt %. C/W ratio obtained = 0.79 ± 0.1.

Reaction of TBE with [≡Si−O−Zr(Np)$_3$]. To understand the role of the second metal (here zirconium), we reacted silica-supported zirconium [≡Si−O−Zr(Np)$_3$] with *n*-decane and TBE and heated it at 150 °C. At the end of the reaction, GC and GC−MS data confirm the formation of olefin (2,2-dimethyldec-3-ene) from *n*-decane.

Typical Procedure for *n*-Decane Metathesis Reactions. A mixture of **4**, **6**, and **7** (1.23 × 10^{-3} mmol of W) and dry *n*-decane (5.14 mmol) was mixed inside the glovebox. The ampules were sealed under vacuum, immersed in an oil bath, and heated at 150 °C. At the end of the reaction, the ampules were frozen using liquid nitrogen. Then, the catalytic run was quenched by addition of a fixed amount of CH_2Cl_2, and after filtration, the resulting solution was analyzed by GC and GC/MS. For kinetic studies, each analysis represents an independent run.

DOI: 10.1021/jacs.6b04307
J. Am. Chem. Soc. 2016, 138, 8595−8602

■ ASSOCIATED CONTENT

Supporting Information

The Supporting Information is available free of charge on the ACS Publications website at DOI: 10.1021/jacs.6b04307.

IR spectra of **4**, solution NMR spectra of **1** and **2**, solid-state NMR spectra of **6** and **7**, and variable temperature of **4** (PDF)

■ AUTHOR INFORMATION

Corresponding Authors

*jeanmarie.basset@kaust.edu.sa

*manoja.samantaray@kaust.edu.sa

Notes

The authors declare no competing financial interest.

■ ACKNOWLEDGMENTS

The authors acknowledge the KAUST Nuclear Magnetic Resonance Core Lab and analytical core lab (ACL) for the analysis of the sample. This publication is based upon work supported by the King Abdullah University of Science and Technology (KAUST) Office of Sponsored Research (OSR).

■ REFERENCES

(1) Pelletier, J. D. A.; Basset, J. M. *Acc. Chem. Res.* **2016**, *49*, 664.

(2) Basset, J. M.; Coperet, C.; Soulivong, D.; Taoufik, M.; Cazat, J. T. *Acc. Chem. Res.* **2010**, *43*, 323.

(3) Coperet, C.; Comas-Vives, A.; Conley, M. P.; Estes, D. P.; Fedorov, A.; Mougel, V.; Nagae, H.; Nunez-Zarur, F.; Zhizhko, P. A. *Chem. Rev.* **2016**, *116*, 323.

(4) Haibach, M. C.; Kundu, S.; Brookhart, M.; Goldman, A. S. *Acc. Chem. Res.* **2012**, *45*, 947.

(5) Basset, J. M.; Coperet, C.; Soulivong, D.; Taoufik, M.; Thivolle-Cazat, J. *Angew. Chem., Int. Ed.* **2006**, *45*, 6082.

(6) Labinger, J. A.; Bercaw, J. E. *Nature* **2002**, *417*, 507.

(7) Basset, J. M.; Coperet, C.; Lefort, L.; Maunders, B. M.; Maury, O.; Le Roux, E.; Saggio, G.; Soignier, S.; Soulivong, D.; Sunley, G. J.; Taoufik, M.; Thivolle-Cazat, J. *J. Am. Chem. Soc.* **2005**, *127*, 8604.

(8) Burnett, R. L.; Hughes, T. R. *J. Catal.* **1973**, *31*, 55.

(9) Goldman, A. S.; Roy, A. H.; Huang, Z.; Ahuja, R.; Schinski, W.; Brookhart, M. *Science* **2006**, *312*, 257.

(10) Huang, Z.; Rolfe, E.; Carson, E. C.; Brookhart, M.; Goldman, A. S.; El-Khalafy, S. H.; MacArthur, A. H. R. *Adv. Synth. Catal.* **2010**, *352*, 125.

(11) Vidal, V.; Theolier, A.; ThivolleCazat, J.; Basset, J. M. *Science* **1997**, *276*, 99.

(12) Szeto, K. C.; Hardou, L.; Merle, N.; Basset, J. M.; Thivolle-Cazat, J.; Papaioannou, C.; Taoufik, M. *Catal. Sci. Technol.* **2012**, *2*, 1336.

(13) Coperet, C.; Maury, O.; Thivolle-Cazat, J.; Basset, J. M. *Angew. Chem., Int. Ed.* **2001**, *40*, 2331.

(14) Le Roux, E.; Taoufik, M.; Baudouin, A.; Coperet, C.; Thivolle-Cazat, J.; Basset, J. M.; Maunders, B. M.; Sunley, G. J. *Adv. Synth. Catal.* **2007**, *349*, 231.

(15) Taoufik, M.; Le Roux, E.; Thivolle-Cazat, J.; Coperet, C.; Basset, J. M.; Maunders, B.; Sunley, G. J. *Top. Catal.* **2006**, *40*, 65.

(16) Le Roux, E.; Chabanas, M.; Baudouin, A.; de Mallmann, A.; Coperet, C.; Quadrelli, E. A.; Thivolle-Cazat, J.; Basset, J. M.; Lukens, W.; Lesage, A.; Emsley, L.; Sunley, G. J. *J. Am. Chem. Soc.* **2004**, *126*, 13391.

(17) Chen, Y.; Abou-hamad, E.; Hamieh, A.; Hamzaoui, B.; Emsley, L.; Basset, J. M. *J. Am. Chem. Soc.* **2015**, *137*, 588.

(18) Blanc, F.; Coperet, C.; Thivolle-Cazat, J.; Basset, J. M. *Angew. Chem., Int. Ed.* **2006**, *45*, 6201.

(19) Saint-Arroman, R. P.; Chabanas, M.; Baudouin, A.; Coperet, C.; Basset, J. H.; Lesage, A.; Emsley, L. *J. Am. Chem. Soc.* **2001**, *123*, 3820.

(20) Le Roux, E.; Taoufik, M.; Coperet, C.; de Mallmann, A.; Thivolle-Cazat, J.; Basset, J. M.; Maunders, B. M.; Sunley, G. J. *Angew. Chem., Int. Ed.* **2005**, *44*, 6755.

(21) Samantaray, M. K.; Callens, E.; Abou-Hamad, E.; Rossini, A. J.; Widdifield, C. M.; Dey, R.; Emsley, L.; Basset, J. M. *J. Am. Chem. Soc.* **2014**, *136*, 1054.

(22) Samantaray, M. K.; Dey, R.; Abou-Hamad, E.; Hamieh, A.; Basset, J. M. *Chem. - Eur. J.* **2015**, *21*, 6100.

(23) Corker, J.; Lefebvre, F.; Lecuyer, C.; Dufaud, V.; Quignard, F.; Choplin, A.; Evans, J.; Basset, J. M. *Science* **1996**, *271*, 966.

(24) Besedin, D. V.; Ustynyuk, L. Y.; Ustynyuk, Y. A.; Lunin, V. V. *Top. Catal.* **2005**, *32*, 47.

(25) Quignard, F.; Lecuyer, C.; Choplin, A.; Olivier, D.; Basset, J. M. *J. Mol. Catal.* **1992**, *74*, 353.

(26) Maity, N.; Barman, S.; Callens, E.; Samantaray, M. K.; Abou-Hamad, E.; Minenkov, Y.; D'Elia, V.; Hoffman, A. S.; Widdifield, C. M.; Cavallo, L.; Gates, B. C.; Basset, J. M. *Chem. Sci.* **2016**, *7*, 1558.

(27) Rataboul, F.; Baudouin, A.; Thieuleux, C.; Veyre, L.; Coperet, C.; Thivolle-Cazat, J.; Basset, J. M.; Lesage, A.; Emsley, L. *J. Am. Chem. Soc.* **2004**, *126*, 12541.

(28) Gregson, D.; Howard, J. A. K.; Nicholls, J. N.; Spencer, J. L.; Turner, D. G. *J. Chem. Soc., Chem. Commun.* **1980**, 572.

(29) Schrock, R. R.; Shih, K. Y.; Dobbs, D. A.; Davis, W. M. *J. Am. Chem. Soc.* **1995**, *117*, 6609.

(30) Dobbs, D. A.; Schrock, R. R.; Davis, W. M. *Inorg. Chim. Acta* **1997**, *263*, 171.

(31) Domski, G. J.; Rose, J. M.; Coates, G. W.; Bolig, A. D.; Brookhart, M. *Prog. Polym. Sci.* **2007**, *32*, 30.

(32) Pfennig, V.; Seppelt, K. *Science* **1996**, *271*, 626.

(33) Shortland, A.; Wilkinson, G. *J. Chem. Soc., Dalton Trans.* **1973**, 872.

(34) Saint-Arroman, R. P.; Basset, J. M.; Lefebvre, F.; Didillon, B. *Appl. Catal., A* **2005**, *290*, 181.

(35) Sommer, W.; Gottwald, J.; Demco, D. E.; Spiess, H. W. *J. Magn. Reson., Ser. A* **1995**, *113*, 131.

■ NOTE ADDED AFTER ASAP PUBLICATION

This paper was published on June 28, 2016. Due to a production error, Scheme 2 was incomplete. The scheme has been updated and the revised version was re-posted on July 13, 2016.

DOI: 10.1021/jacs.6b04307
J. Am. Chem. Soc. 2016, 138, 8595−8602